Journal of Hydrology 566 (2018) 818–829

Contents lists available at ScienceDirect

Journal of Hydrology

journal homepage: www.elsevier.com/locate/jhydrol

Research papers

Assessing hydrological impacts of short-term climate change in the Mara River basin of East Africa

Tirthankar Roy[a,b,*], Juan B. Valdés[a], Bradfield Lyon[c,d], Eleonora M.C. Demaria[e], Aleix Serrat-Capdevila[f], Hoshin V. Gupta[a], Rodrigo Valdés-Pineda[a], Matej Durcik[g]

[a] Hydrology and Atmospheric Sciences, The University of Arizona, Tucson, United States
[b] Civil and Environmental Engineering, Princeton University, Princeton, United States
[c] Climate Change Institute, The University of Maine, Orono, United States
[d] International Research Institute for Climate and Society, Columbia University, Palisades, United States
[e] USDA Agricultural Research Service, Tucson, United States
[f] Water Global Practice, The World Bank, Washington, DC, United States
[g] Biosphere 2, The University of Arizona, Tucson, United States

ARTICLE INFO

This manuscript was handled by A. Bardossy, Editor-in-Chief, with the assistance of Purna Chandra Nayak, Associate Editor

Keywords:
Short-term climate change impacts
VARAG data
Natural climate variability
Bias correction
VIC model
Mara River basin

ABSTRACT

We assess the impacts of a range of short-term climate change scenarios (2020–2050) on the hydrology of the Mara River Basin in East Africa using a new high-resolution (0.25°) daily climate dataset. The scenarios combine natural climate variability, as captured by a vector autoregressive (VAR) model, with a range of climate trends calculated from 31 models in the Coupled Model Intercomparison Project Phase 5 (CMIP5). The methodology translates these climate scenarios into plausible daily sequences of climate variables utilizing the Agricultural Modern-Era Retrospective Analysis for Research and Applications (AgMERRA) dataset. The new dataset (VARAG) has several advantages over traditional general circulation model outputs, such as, the statistical representation of short-term natural climate variability, availability at a daily time scale and high spatial resolution, not requiring additional downscaling, and the use of the AgMERRA data which is bias-corrected extensively. To assess the associated impacts on basin hydrology, the semi-distributed Variable Infiltration Capacity (VIC) land-surface model is forced with the climate scenarios, after being calibrated for the study area using the fine-resolution (0.05°) merged satellite and in-situ observation-based dataset, Climate Hazards Group InfraRed Precipitation with Station data (CHIRPS). The climate data are further bias-corrected by applying a non-parametric quantile mapping scheme, where the cumulative distribution functions are approximated using kernel densities. Three different wetness scenarios (*dry*, *average*, and *wet*) are analyzed to see the potential short-term changes in the basin. We find that the precipitation bias correction is more in effect in the mountainous sub-basins, one of which also shows the maximum difference between the wet and dry scenario streamflows. Precipitation, evapotranspiration, and soil moisture show increasing trends mostly during the primary rainy season, while no trend is found in the corresponding streamflows. The annual values of these variables also do not change much in the coming three decades. The methodology implemented in this study provides a reliable range of possibilities which can greatly benefit risk analysis and infrastructure designing, and shows potential to be applied to other basins.

1. Introduction

Although challenging, the assessment of the hydrological impacts of climate change is necessary for medium- to long-term water resources planning and management, design of future adaptation strategies, and resilience building. Such assessments typically use downscaled global circulation model (GCM) outputs to drive hydrologic models, under plausible assumptions regarding different greenhouse gas (GHG) emission scenarios. In doing so, it is important to consider the potential sources of uncertainties associated with various components within the modeling framework; for example, uncertainties in GCM outputs due to inadequate representation of climate system physics, observational uncertainties in the evaluation data, process parameterizations, land-use change, greenhouse gases, aerosol emissions, etc. (Flato et al.,

* Corresponding author at: Civil and Environmental Engineering, Princeton University, Princeton, New Jersey, United States.
E-mail address: royt@email.arizona.edu (T. Roy).

https://doi.org/10.1016/j.jhydrol.2018.08.051
Received 12 March 2018; Received in revised form 2 August 2018; Accepted 24 August 2018
Available online 27 August 2018
0022-1694/

2013) or uncertainties in the representation of structural and functional aspects of the hydrologic system (Allen et al., 2006; Gupta et al., 2012), and so on.

Further, because the spatial resolution of GCM outputs is typically too coarse for hydrologic applications, such outputs are often mapped to higher resolution using statistical or dynamical downscaling (see recent review by Teutschbein et al. (2011). However, because these outputs tend to exhibit bias when compared against some "ground truth", correction strategies must be applied (see recent review by Teutschbein and Seibert, 2012). Established methods for bias correction include quantile mapping or distribution mapping (Panofsky and Brier, 1968; Wood et al., 2002; Snover et al., 2003; Yuan and Wood, 2012), where the probability distribution of the raw data is mapped to the reference data.

In addition to the uncertainties associated with GCM outputs, the time horizons also play a key role in determining the reliability of the climate model outputs. At shorter time horizons (e.g. decades) the predictability of atmosphere-ocean system is greatly reduced (Boer and Lambert, 2008; Teng and Branstator, 2011; Greene et al., 2012). Furthermore, the natural variability of climate contributes substantially to interannual climate fluctuations, particularly for shorter time horizons (Greene et al., 2011). Interestingly, from the perspective of water allocation planning and resources management, the shorter time horizons are of more immediate relevance (Greene et al., 2012).

The Mara River basin in East Africa has been experiencing high water demand in recent times, because of which, the available water resources are often being over-exploited (Dessu et al., 2014). Consequently, effective water resources planning and management, especially at shorter time horizons, is an indispensable need in the basin. Decadal forecasts of different hydroclimatic variables are crucial for addressing the substantial water problems in the basin. To date, only a very few studies have attempted climate impact assessments for the basin. Mati et al. (2008) studied the impacts of agricultural expansion on Mara River streamflow during the 1973–2000 period, and reported that reduced forest cover has caused flood peak magnitudes to increase. These changes were accompanied by enhanced upstream soil erosion and increased downstream build-up of silt. Mango et al. (2011) evaluated the potential combined impacts of climate change and land use change in the upper Mara River basin, and concluded that conversion of forests to agriculture and grassland is likely to cause peak flows to increase and dry season (June to September, January to February) flows to decrease, eventually leading to greater water scarcity and hillslope erosion. Defersha et al. (2012) studied watershed-scale sediment yield and runoff response, and found (as expected) that cultivated lands have much higher erosion rates than bush land or grassland. Dessu and Melesse (2012) used climate projections from five GCMs for three different GHG emission scenarios to assess and characterize the uncertainty in climate change impacts, and reported that a statistically significant increase in flow volume can be expected at Mara Mine (discharge station) from 2046 to 2065 to 2081–2100. Overall, these studies suggest the following: (1) significant land-use change from forest to agriculture in the upstream portion of the basin, (2) increased magnitude of flood peaks, (3) decreased dry season flow, (4) greater water scarcity, (5) increased upstream soil erosion, and (6) increased downstream sedimentation.

In this study, we prepare a new climate dataset which combines natural climate variability with temporal trends resulting from increasing greenhouse gases. Natural variability on the seasonal time scale is estimated using the vector autoregressive (VAR) modeling-based approach of Greene et al. (2012), where historical climate observations are used to fit the parameters of the model, which is subsequently used to generate hundreds of plausible, synthetic time series of natural climate variations in the basin. Seasonal climate trends (precipitation, maximum, and minimum temperature) are calculated from an ensemble of 31 models from the Coupled Model Intercomparison Project Phase 5 (CMIP5, Taylor et al., 2012). These trends are then imposed on the synthetic time series of natural variability to generate a full range of plausible seasonal climate change projections for the study area. Of course, an additional source of uncertainty comes from the ability of the CMIP5 models to properly capture the response to increasing greenhouse gas concentrations, given known model deficiencies in simulating the current climate of East Africa (Yang et al., 2014, 2015; Lyon and Vigaud, 2017), which is an important caveat to keep in mind. Once obtained, the seasonal projections are temporally disaggregated to the daily time step, making use of the high resolution (0.25° lat/lon) Agricultural Modern-Era Retrospective Analysis for Research and Applications (AgMERRA) climate data (Ruane et al., 2015). Hereafter, the derived daily time sequences of climate variables will be termed as VARAG (**VAR** approach with **Ag**MERRA). Three different precipitation scenarios (mean/average, 5th percentile/dry, and 95th percentile/wet) are then bias-corrected using a nonparametric quantile mapping scheme with a fine-resolution satellite and in-situ observation-based merged dataset, Climate Hazards Group InfraRed Precipitation with Station data (CHIRPS; Funk et al., 2014, Funk et al., 2015), as the reference. The bias-corrected daily climate projections are then used as forcings to the land-surface model, Variable Infiltration Capacity (VIC; Liang et al., 1994), which is calibrated using the SCE-UA algorithm (Duan et al., 1992, Duan et al., 1993), to generate plausible hydrological projections for the basin.

The main objective of this study is to address two main research questions:

(1) How do the VARAG precipitation scenarios (dry, average, and wet) compare with the climatology of basin precipitation?
(2) What are the impacts of different short-term/near-term VARAG precipitation scenarios on basin hydrology?

2. Study area

The 13,504 km^2 transboundary Mara River basin (Location: 33°88′E to 35°90′E & 0°28′S to 1°97′S) has about 65% of its area in Kenya and 35% in Tanzania, Africa. The Nyangores and Amala rivers originate at the Mau Forest Escarpment (3000 m ASL) and merge at the Napuiyapi swamp (2932 m ASL) to create the Mara River, which flows 395 km to its mouth at the Musoma Bay, Lake Victoria, Tanzania (1130 m above MSL). Being the only perennial river in the region, the Mara River plays an important role in the ecohydrology of the basin (McClain et al., 2014).

The climatology of the basin precipitation is bimodal due to sub-annual translation of the intertropical convergence zone (ITCZ), with the main rainy season from March to May and the secondary season from October to November. Long-term mean annual precipitation varies from 600 mm to 1500 mm (McClain et al., 2014).

About one million people live in the Mara basin, where the main socioeconomic activity is crop farming, followed by livestock rearing, tourism, and wildlife sanctuary (Mati et al., 2005). Due to population growth and agricultural expansion, the basin has experienced a very high rate of deforestation, with almost 4500 km^2 (approximately one-third of the basin) having been transformed into farmland and tea plantations by 2000 (Mati et al., 2005; McClain et al., 2014). The basin encompasses the Masai-Mara National Reserve (Kenya) and the Serengeti National Park along with game reserves (in Tanzania) that attract thousands of tourists due to the rich biodiversity and the annual mass migration of millions of animals.

In this study, we focus on the Mara River basin and its five sub-basins (Fig. 1, Supporting Information Table S1). Two sub-basins in the northeast encompass the Nyangores and Amala tributaries. Three sub-basins in the east encompass the Lemek, Talek, and Sand tributaries. All the five sub-basins drain into the mid region of the basin, referred to as Mid-Mara. Discharge data are only available at three discharge stations: Bomet Bridge (Nyangores River), Kapkimolwa Bridge (Amala River), and Mara Mine (Mara River). Although no ground-based streamflow

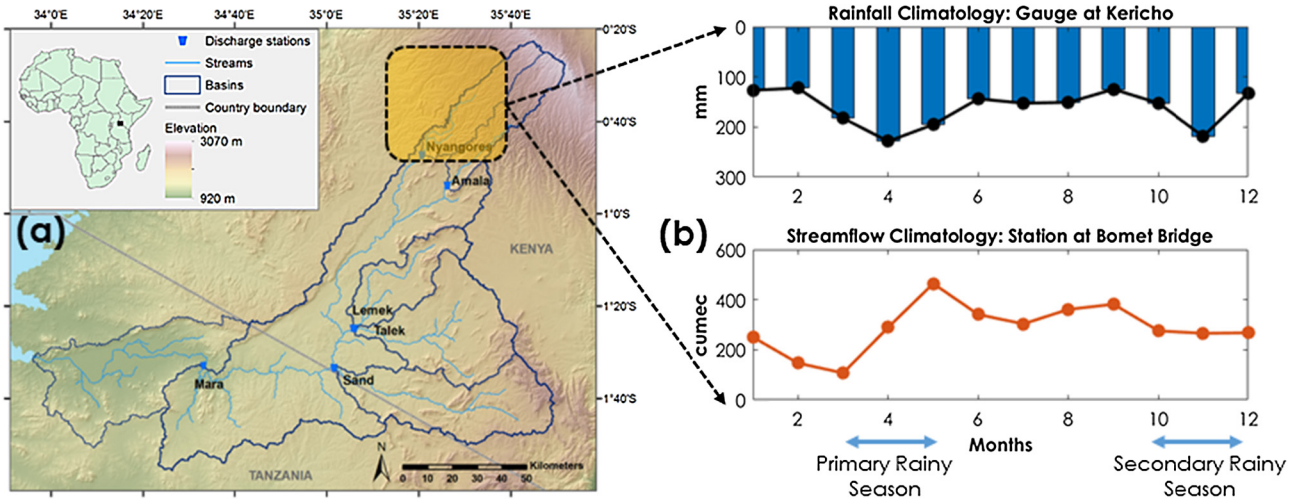

Fig. 1. (a) The Mara River basin and its sub-basins. Watershed outlets are shown in blue. All other outlets except Mara Mine are located in Kenya, while the latter is located in Tanzania. (b) The climatology of precipitation (Raingauge at Kericho near Nyangores sub-basin) and streamflow (Discharge station at Bomet Bridge in Nyangores sub-basin). (For interpretation of the references to colour in this figure legend, the reader is referred to the web version of this article.)

records are available for the other three sub-basins, they play crucial roles in the water management of the region.

3. Methodology

3.1. Datasets

This study involves multiple datasets at different stages. Climate change projections for the basin were derived using the University of East Anglia Climate Research Unit (CRU; Harris et al., 2014) monthly precipitation and temperature (version TS3.2) data, precipitation projections from 31 climate models contained in the CMIP5 archive using the RCP8.5 radiative forcing scenario, and AgMERRA data. The bias correction of the climate data as well as the calibration of the hydrologic mode VIC were carried out using the Climate Hazards Group InfraRed Precipitation with Station (CHIRPS) dataset, which combines both satellite estimates and in-situ measurements. Temperature and wind speed data for the VIC model calibration were derived from the National Centers for Environmental Information (NCEI) meteorological station data archive (formerly known as NCDC: National Climatic Data Center). The observed streamflow data were collected from the local water management authority.

3.1.1. AgMERRA climate forcings

The AgMERRA dataset combines NASA's MERRA reanalyses data (Rienecker et al., 2011) with in-situ and remotely-sensed observations of precipitation, temperature, and solar radiation to produce daily high resolution (0.25˚) fields of climate forcing data with significantly reduced bias (Ruane et al., 2015*)* relative to observations from 2324 stations in the Hadley Integrated Surface Dataset (HadISD; Dunn et al., 2012). The product has been shown to compare well with several contemporary forcing datasets, including the Princeton Climate Forcing Dataset (Sheffield et al., 2006), the Water and Global Change (WATCH) Forcing Dataset (WFD; Weedon et al., 2011), WFD with ERA-Interim (WFD-EI; Weedon et al., 2011), and the meteorological forcing dataset the Global Risk Assessment for the Stable Production of Food (GRASP; Iizumi et al., 2014). Additionally, AgMERRA incorporates the MERRA-Land dataset (Reichle, 2012), which includes Climate Prediction Center's Unified precipitation product (Chen et al., 2008), resulting in significantly improved representation of daily precipitation and extreme events. The dataset also incorporates three high resolution satellite-based precipitation estimates, namely Tropical Rainfall Measuring Mission (TRMM) 3B42 (Huffman et al., 2007), Precipitation Estimation using Remote-Sensing and Artificial Neural Networks (PERSIANN; Hsu et al., 1997), and Climate Prediction Center Morphing Technique (CMORPH; Joyce et al., 2004).

3.1.2. VARAG future climate forcings

In the coming decades, interannual climate fluctuations associated with natural variability could be a major contributor to hydrologic variations in many regions around the globe (Greene et al., 2011). Such natural variations can also affect short-term (e.g. 30-year) climate trends and thus, projections of near-term climate change. To address this issue, we follow the methodology of Greene et al. (2012), where we combine information regarding natural climate variations based on observational data, with climate model projections used to quantify trends under increased greenhouse gas forcing.

Fig. 2 shows the main steps involved in the data preparation technique. The first step was to extract seasonal average CRU precipitation data along with maximum and minimum temperature data (1901–2013) for a rectangular region (2.5˚S-0˚N, 33.5˚E-36.5˚E) that includes the Mara Basin. Only the wet seasons of March-May and October-December were used in the VAR model. The three variables were then regressed onto the global average surface temperature time series obtained from the average of 31 CMIP5 climate model simulations that include increasing greenhouse gases, and therefore constitute the anthropogenic signal. The regressed relationships were used to de-trend the original CRU time series data (they are subtracted from the original data), generating residual values for each variable that constitute natural climate variability. The detrended time series (seasonal precipitation and maximum and minimum temperature) were then used to fit the parameters of the VAR model that captures both the autocorrelation of each of the three variables as well as the covariance among them.

Once the model parameters were determined, the VAR model was used to generate 200, synthetic climate scenario time series consisting of seasonal average values 31 years in length (representing 2020–2050). Linear trends from 2020 to 2050 in the three variables were then computed for the region based on 31 CMIP5 model projections run under the RCP8.5 scenario representing extreme greenhouse gas emissions *(*Riahi et al., 2011*)*. From the 31 computed trends, the four representing the mean, 5th, 50th, and 95th percentile values were selected. These four trend scenarios were then superimposed on each of the 200 synthetic climate simulations to generate what is considered the full range of plausible climate change projections for the basin (trend from CMIP5 and natural variability from the VAR). For each of these four sets of 200 scenarios, the seasonal precipitation averaged

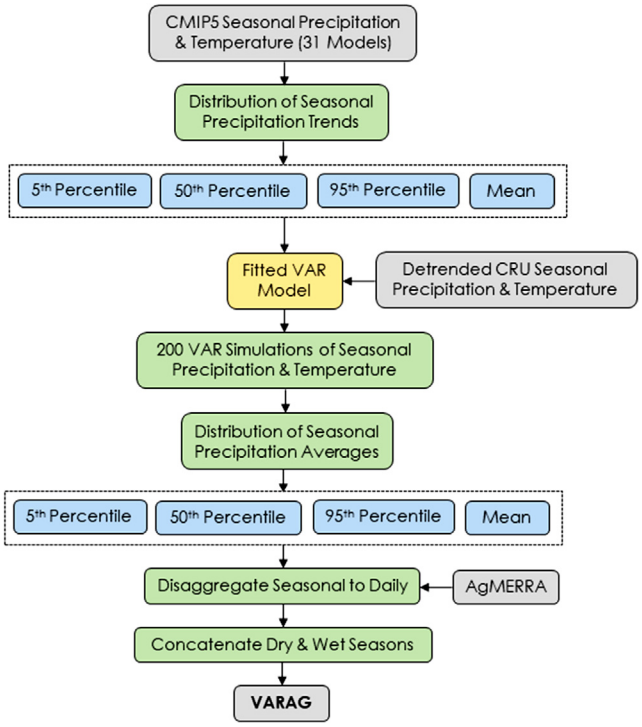

Fig. 2. VARAG preparation flow chart.

over the period 2020–2050 was determined for each set, and the mean, 5th, 50th and 95th percentile values were identified. For example, in the case of the 5th percentile trend imposed from CMIP5, the 5th percentile of seasonal mean rainfall for 2020–2050 was selected from the 200 superimposed time series. The purpose of this was to capture how natural variability can either enhance or reduce the imposed trend just by chance. As the historical March-May and October-December rainfall seasons in the Mara Basin do not show a statistically significant relationship to one another, climate scenarios for the March-May and October-December seasons were computed separately in our approach. These seasons were subsequently concatenated with the intervening dry seasons (January-February, June-September), where the dry seasons for an individual year was chosen randomly from the AgMERRA data. The seasonal temperature trends from the CMIP5 model projections were added to the temperature time series from VAR for all seasons (i.e. including the dry seasons). Thus, we derived 31-year climate projections for the Mara Basin covering the period 2020–2050 based on the seasonal data.

To disaggregate the synthetic seasonal climate scenarios down to plausible daily weather sequences, a k-nearest neighbor approach was employed. Using all three scenario variables (precipitation, maximum, and minimum temperature) for a given season and year, the three-nearest neighbors in seasonal averages of the AgMERRA data were identified. To add a stochastic element, a single nearest neighbor was chosen from the three using a random process with unequal weighting, with the largest weighting applied to the first nearest neighbor. The difference in seasonal temperature between the scenario value and AgMERRA nearest neighbor was then computed for each season of each year. For precipitation, the ratio of the two precipitation values was computed. The daily AgMERRA values, for each identified season and year and for each grid point within the Mara Basin, then served as a plausible daily sequence within the season. To have the AgMERRA data exactly match that of the seasonal value of the climate scenario, the difference (between seasonal scenario and AgMERRA) in seasonal maximum and minimum temperature was added to each daily AgMERRA value, while for precipitation, multiplicative adjustment was used. The end result was a sequence of daily forcing values covering the period 1 January 2020 to 31 December 2050 for four different wetness scenarios (mean and the 5th, 50th, 95th percentiles).

3.1.3. CHIRPS precipitation

The Climate Hazards Group InfraRed Precipitation with Station data (CHIRPS; Funk et al., 2014, Funk et al., 2015) is a satellite-based quasi-global (50° N-S, 180° W-E) merged precipitation dataset available from 1981 to near-present (~1 month latency). CHIRPS incorporates information from five different sources; (1) pentadally (5-day) disaggregated monthly precipitation climatology (CHPClim), (2) quasi-global geostationary thermal-IR satellite observations from two NOAA sources (CPC IR & NCDC B1 IR), (3) TRMM-3B42 precipitation estimates, (4) precipitation fields from NOAA Climate Forecast System, version 2 (CFSv2), and (5) in-situ precipitation observations both from national and regional sources (CHG Station Climatology Database, UCSB). The latest version of CHIRPS (version 2) with 0.05° × 0.05° spatial and daily temporal resolutions is used in this study.

As per the CHIRPS algorithm, cold cloud top (< 235° K) duration is calculated first as the percent of pentad, i.e., the percent of time during the pentad that corresponds to the cold could top. Then, predetermined local regression equations based on TRMM 3B42 pentad rainfall estimates are used to convert this duration into mm of precipitation. The percent of normal pentad precipitation is calculated by dividing the pentad values by their long-term means, which is then multiplied by the Climate Hazards Group's Precipitation Climatology (CHPClim) pentad to produce unbiased gridded precipitation estimates. Finally, for each grid location, five nearest station observations are assimilated using weights that are proportional to the square of the correlation coefficients, thereby producing the CHIRPS estimates.

3.1.4. Station Data: temperature, wind speed, and discharge

The Global Surface Summary of the Day (GSOD) products produced by the National Climatic Data Center (NCDC) in Asheville, NC (currently a part of NCEI), are used in this study as the in-situ observations of precipitation, temperature (maximum, minimum, and average), and wind speed. Six of the total available stations had relatively good coverage and so they were used for this study. Discharge data were available for three sub-basins out of six (Nyangores at Bomet Bridge, Amala at Kapkimolwa, and Mara at Mara Mine) with different temporal coverages (see Supporting Information Table S2). Streamflow values are based on calibrated stage-discharge relationships fed with stage measurements. The uncertainty in the stage to discharge transformation was not accounted for in this study.

3.2. Hydrologic model VIC

The VIC model (Liang et al., 1994) is a physically-based semi-distributed hydrologic model that can solve both water and energy budget equations simultaneously; for this study, the model was run in water budget mode at a daily time step and a 0.05° spatial resolution. Independent calculations are carried out at each grid cell, and the model accounts for sub-grid heterogeneity in a statistical manner. VIC requires that at least four inputs be provided (precipitation, maximum air temperature, minimum air temperature, and wind speed) and, unless provided explicitly, all other required variables are derived within the model from these four inputs (see Supporting Information Table S3). The model consists of three soil layers and a thin canopy layer on the top. Horizontal routing within the model is a two-step process. *First*, the runoff from each grid cell is routed from that cell to the channel using a triangular unit hydrograph. *Second*, the water in the channel is routed to the outlet using the linearized St. Venant's equations (Lohmann et al., 1996, Lohmann et al., 1998). Six parameters of the model were calibrated in this study (see Supporting Information Table S4); these are the ones suggested by the developers as being the most sensitive (Information retrieved from:

www.hydro.washington.edu/Lettenmaier/Models/VIC/

Documentation/Calibration.shtml#General.Last accessed: Sept 18, 2018).

3.3. Model calibration

Discharge data from the three gauge stations (Bomet, Kapkimolwa, and Mara Mine) did not share a common time frame (Supporting Information Table S2). Therefore, to make the best use of the available data, step-wise calibration was performed using different calibration and evaluation periods for each sub-basin. Calibration was carried out individually using distributed forcing, and the same calibrated parameters were applied in all grid cells. The Nyangores and Amala sub-basins were calibrated first individually for their respective outlet points at Bomet and Kapkimolwa. Next, the Mara basin was calibrated using the discharge data from the outlet point at Mara Mine. The final parameter file was prepared by combining the three different sets of parameters corresponding to Nyangores, Amala, and Mara. The Shuffled Complex Evolution-University of Arizona (SCE-UA; Duan et al., 1992, Duan et al., 1993) optimization algorithm was used for calibrating the model parameters at a daily time step using CHIRPS as the precipitation forcing. The mean squared error of the transformed (Box and Cox, 1964) flows was used as the objective function to be minimized. The λ-parameter of the transformation equation was calculated from the observed streamflow values such that it minimizes the skewness (Roy et al., 2017a, 2017b). For the ungauged sub-basins (Lemek, Talek, and Sand), calibrated parameters of the Mara basin were implemented. Note that the quality of streamflow observations was not up to the mark for Kapkimolwa Bridge and Mara Mine stations, however, we still wanted to utilize all the resources we had at our disposal. Calibration in the λ-transformed space is particularly useful in this case in order to capture the mean behavior of the observed streamflow time series. This does, however, deteriorate the error statistics. For Bomet Bridge, although the observed hydrograph was captured well by the VIC model, there were few instances of high peaks in the simulated flows, which again deteriorated the error statistics. Calibration results are presented in Supporting Information Table S5.

3.4. Precipitation bias correction

Bias correction of VARAG raw precipitation data was carried at a monthly time scale on a cell-to-cell basis using adjusted CHIRPS as the reference data. The correction scheme followed two steps. First, raw CHIRPS data were slightly adjusted in a lumped manner to match the long-term means of the local National Climatic Data Center (NCDC) rain gauges (see methodology in Roy et al., 2017b). Second, cell-to-cell distributed correction was carried out using a nonparametric quantile mapping approach, where the cumulative distribution functions (CDFs) were approximated by kernel densities. Although the applications of kernel densities are widespread (Rosenblatt, 1956; Silverman, 1981; Sheather and Jones, 1991; Kim et al., 2003), they have not been used widely within the context of quantile mapping-based bias correction. In this method, the probability distributions of the raw and the reference data are approximated by Kernel Densities, which helps overcome several weaknesses associated with the use of purely empirical distributions (e.g. lack of smoothness) or theoretical distributions (e.g. frequent over-smoothing).

Quantile mapping is used to match the distribution quantiles of the raw data (RW) to that of the reference data (RF), thereby producing the bias-corrected data (BC), with statistical properties similar to the reference data. Mathematically, this can be shown as:

$$BC = F_{RF}^{-1}(F_{RW}(RW)) \quad (1)$$

where F_{RW} is the CDF of the raw data and F_{RF}^{-1} is the inverse CDF of the reference data.

The CDFs of raw and reference data are approximated using kernel density functions, which can be expressed as:

$$\hat{f}(x) = \frac{1}{nb}\sum_{i=1}^{n} K\left(\frac{x_i - x}{b}\right) \quad (2)$$

where $\hat{f}(x)$ is the estimated density at point $\boldsymbol{x}$, x_i is the sample point at i^{th} location, n is the total number of sample points, K is the kernel, and b is the bandwidth.

The kernel function represents the influence of adjacent points based on their distance from the evaluation point. As this distance increases, the associated weight decreases. Thus, any sample point probability is characterized by not only the probability at that point, but also by the probability associated with the neighboring points in a continuously decreasing manner (with distance away from the evaluation point) using some kernel function (e.g. triangular, Gaussian, etc.). The bandwidth in kernel density estimation controls the bias-variance trade-off. If the bandwidth is too small, the kernel densities overfit the data, i.e., the variance increases. On the contrary, if the bandwidth is too large, the kernel densities underfit the data, which means that the bias is increased. Here, the bandwidth was adjusted manually. To implement the nonparametric quantile mapping scheme, we used 1D interpolation with nearest neighborhood smoothing on the precipitation values and the cumulative probabilities.

Bias correction of VARAG raw precipitation was carried out on a monthly time-scale, following which, the bias-corrected monthly values were temporally disaggregated to daily level based on precipitation intensities, with the implicit assumption that higher rainfall intensities are associated with larger bias and vice versa. The correction was not implemented on a daily level because the reference CHIRPS data are produced from pentad climatologies, which do not accurately represent the daily variability of precipitation.

4. Results and discussion

4.1. Precipitation characteristics

The comparison between the basin-averaged mean monthly precipitation from AgMERRA and CHIRPS for the time period 1981–2010 (common time frame) for all six sub-basins is shown in Fig. 3. For each case, it also reports the “bias factor”, i.e., the ratio between the long-term means of CHIRPS (reference) and AgMERRA (raw). Bias factors greater than one imply underestimation (in long-term) of AgMERRA and vice versa. As can be seen, the type of bias varies with the case. AgMERRA significantly underestimates precipitation in the mountainous Nyangores and Amala sub-basins, shows slight underestimation for the Mid-Mara region and Sand sub-basin, and slight overestimation for the Talek and Lemek. This is also evident in the empirical CDF plots, where the upper two sub-basins show significant differences (underestimation of AgMERRA), whereas the remaining four sub-basins have very similar probability distribution characteristics.

Next, we compared future precipitation from raw VARAG against historical CHIRPS (Supporting Information Fig. S1) to see whether or not VARAG precipitation is significantly different from AgMERRA precipitation, and if CHIRPS could at all be used as the reference data. We found that the AgMERRA and VARAG precipitation have very similar mean bias and distribution characteristics, which is also the reason why CHIRPS was finalized for bias-correcting the future data.

Fig. 4 shows monthly precipitation distributions and means for (1) basin-averaged rain gauge measurements, (2) CHIRPS precipitation, (3) AgMERRA precipitation, and (4) average wetness VARAG precipitation. As can be seen, the bimodality of Mara rainfall is well represented in all four datasets. The primary rainy season is during March-May and the secondary during October-December. VARAG precipitation has less spread, overall. The plot in the last row shows monthly bias factors corresponding to CHIRPS, AgMERRA, and VARAG, calculated using the rain gauge measurements as the reference (Bias Factor = Reference/Raw). All three products have similar temporal patterns for the bias factor, with AgMERRA and VARAG having the closest match. Overall,

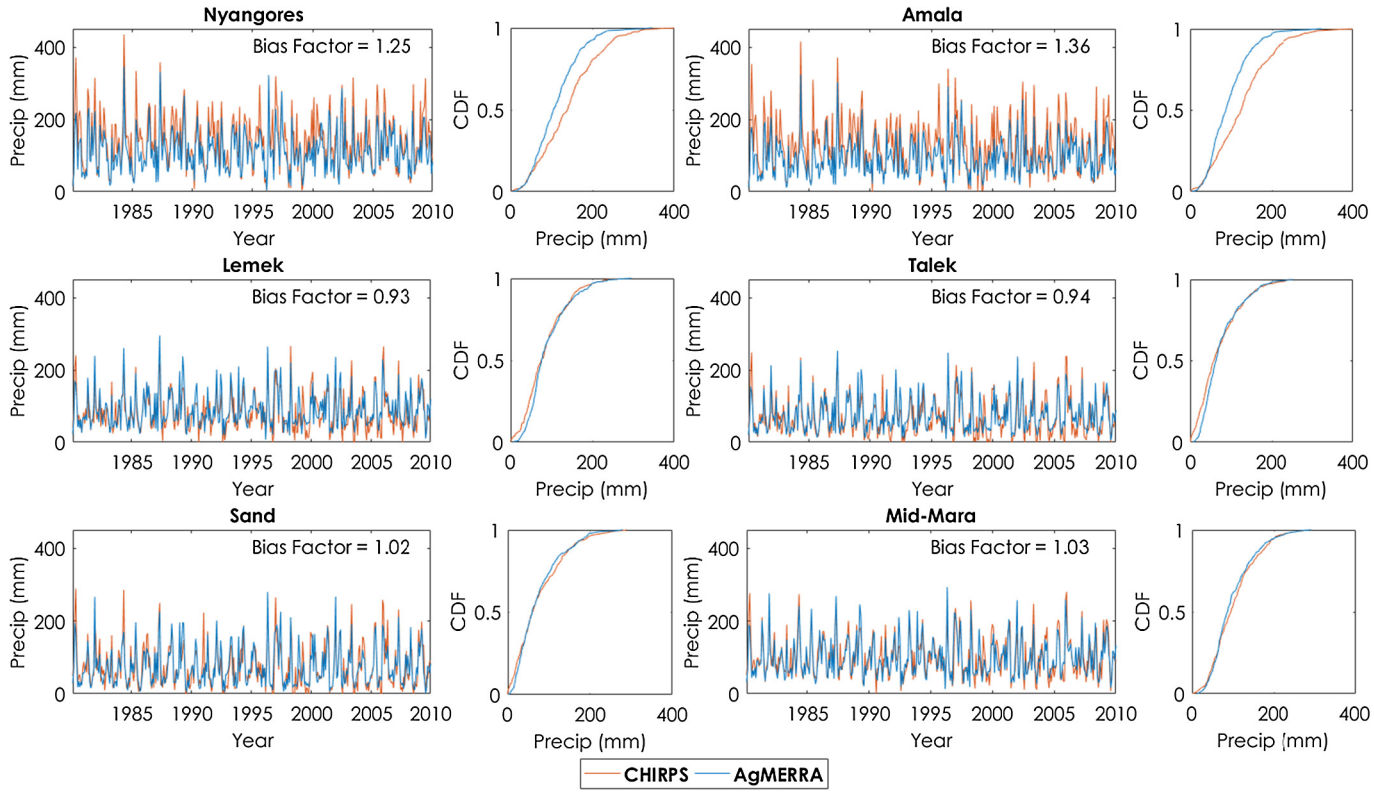

Fig. 3. Monthly precipitation time series (1980–2010) and empirical CDF for the six Mara sub-basins as computed from CHIRPS and AgMERRA. The Bias Factor indicates the ratio between the long-term means of CHIRPS (reference) and AgMERRA (raw).

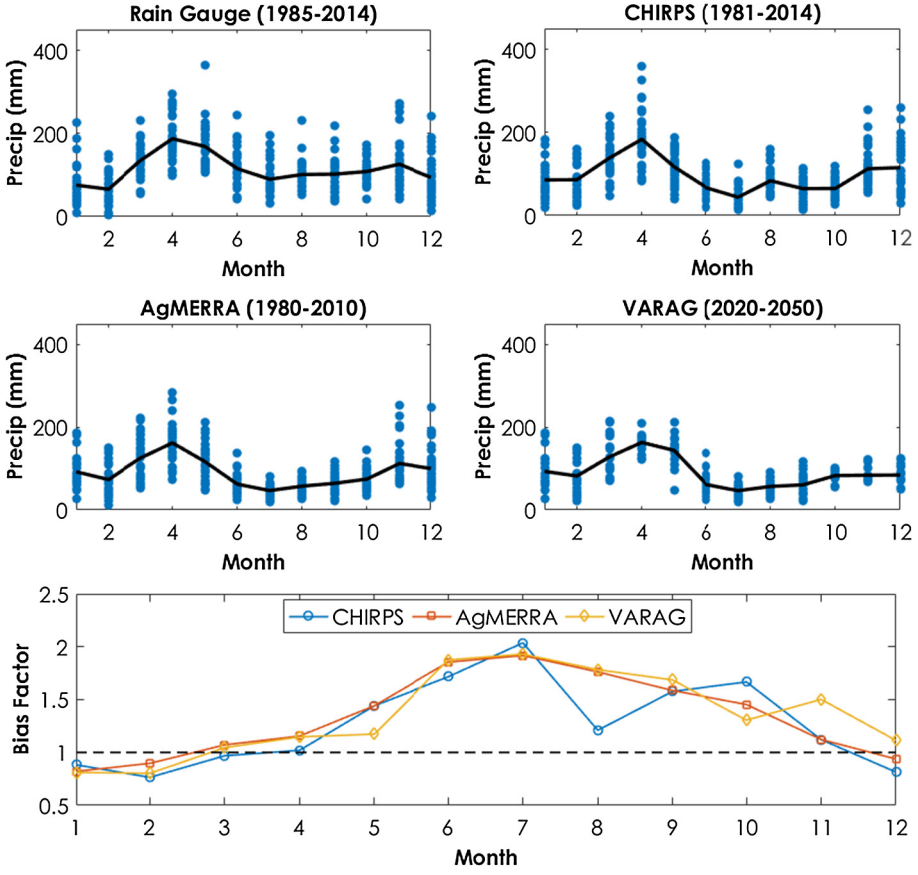

Fig. 4. Comparison of monthly precipitation distributions and means of basin-averaged rain gauge measurements, CHIRPS, AgMERRA, and VARAG.

the bias factor values are closer to 1 during the rainy seasons, and higher during the dry periods, which means, on an average, the dry period precipitation is underestimated by AgMERRA, assuming that the rain gauge measurements during those periods are reasonably accurate. Similar behavior is expected in the future, as demonstrated in VARAG, if we assume stationarity, since the statistical properties are not expected to change significantly within the short time period. It is important to note that the assumption of stationarity is only meaningful when short-term analysis is concerned. For analysis in longer time scales, treatment of nonstationarity becomes crucial.

4.2. Precipitation bias correction

Since the probability distributions of monthly AgMERRA and VARAG precipitation were quite similar (see Fig. 3 and Supporting Information Fig. S1), the bias correction method was first tested with the AgMERRA data for historical time period (1981–2010) to see how closely the bias-corrected values match the reference data (i.e. gauge-adjusted CHIRPS). Bias correction results for four different grid cells from different parts of the Mara River basin are shown in Supporting Information Fig. S2, where the type of bias (whether underestimation or overestimation) is not consistent across the grid cells. The sorted values closely follow the 45° line, indicating that the bias correction has been successful. Fig. 5 presents the bias correction results for the historical time period for the entire study area. Clearly, bias correction scheme has successfully matched all the four moments (mean, standard deviation, skewness, and kurtosis) of the raw monthly AgMERRA data to that of the gauge-adjusted CHIRPS. Note that the use of kernel density functions and the careful selection of the bandwidth value are the key reasons why bias correction has been so efficient in this case. Bias correction results (similar to Fig. 5) of VARAG precipitation are shown in Supporting Information Fig. S3.

4.3. Precipitation projections

Three different future precipitation scenarios (dry, average, and wet) are studied with and without the bias correction (Fig. 6). Assuming that the reference CHIRPS corresponds to average wetness condition, we only bias-correct the average scenario of VARAG. The anomalies of dry and wet scenarios are calculated by subtracting them from the raw means, which are then added back to the corrected means to get the corrected dry and wet scenarios. The negative values produced thereby are all set to zero. Thus, we can have three different scenarios, both before and after the bias correction, which would not be possible had we been bias-correcting all three scenarios directly, because in that case, the bias correction algorithm would consider dryness and wetness as biases and tend to 'correct' them such that they match the mean scenario. This method implicitly assumes that the magnitude of the bias during average wetness conditions is equal during wet and dry conditions.

The accumulated precipitation plots shown in Fig. 6 are useful to detect (1) differences in total precipitation at the end of the analysis period and (2) any drastic change in precipitation over time as reflected by the slope of the curves. As can be seen, none of the six sub-basins showed a noticeable change in the slopes for the different scenarios. Therefore, no drastic change in precipitation is expected in the next three decades. Differences between the dry and wet scenario precipitation at the end of the time period are similar for all six sub-basins, whereas in case of streamflow, these differences are maximum for the mountainous sub-basins. Difference between the dry and wet precipitation scenarios was maximum in the overall basin (199 mm) followed by the Lemek sub-basin (164 mm), and minimum for the Amala sub-basin (130 mm). The effect of bias correction is marginal for Lemek and Talek, where the bias factors are lower than but very close to 1 (0.93 and 0.94, respectively). The slope of the bias-corrected precipitation is always higher for all sub-basins. For Lemek and Talek, again, the increase in slope after bias correction is marginal.

4.4. Hydrologic projections

Hydrologic simulations are carried out for three consecutive decades (2021–2030, 2031–2040, and 2041–2050) using the calibrated

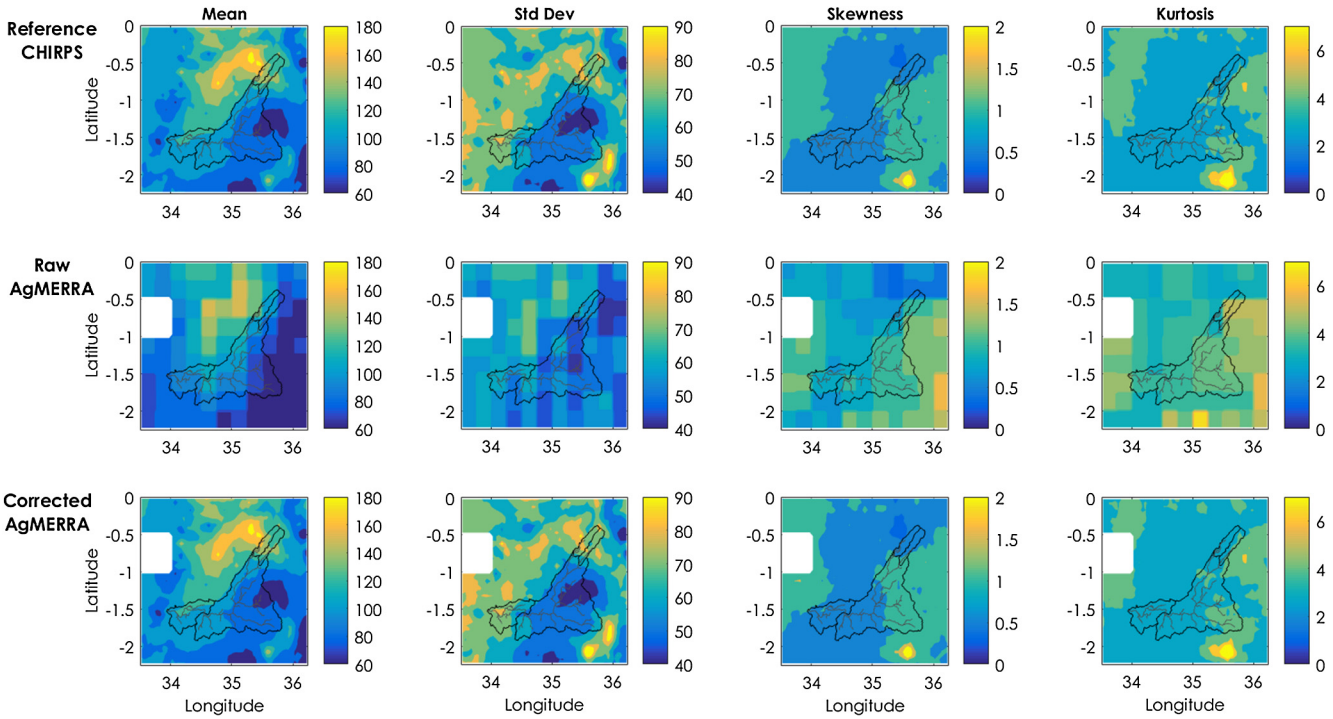

Fig. 5. Spatial plots showing the statistical moments of raw, reference, and bias-corrected monthly AgMERRA precipitation data during the historical period (1981–2010).

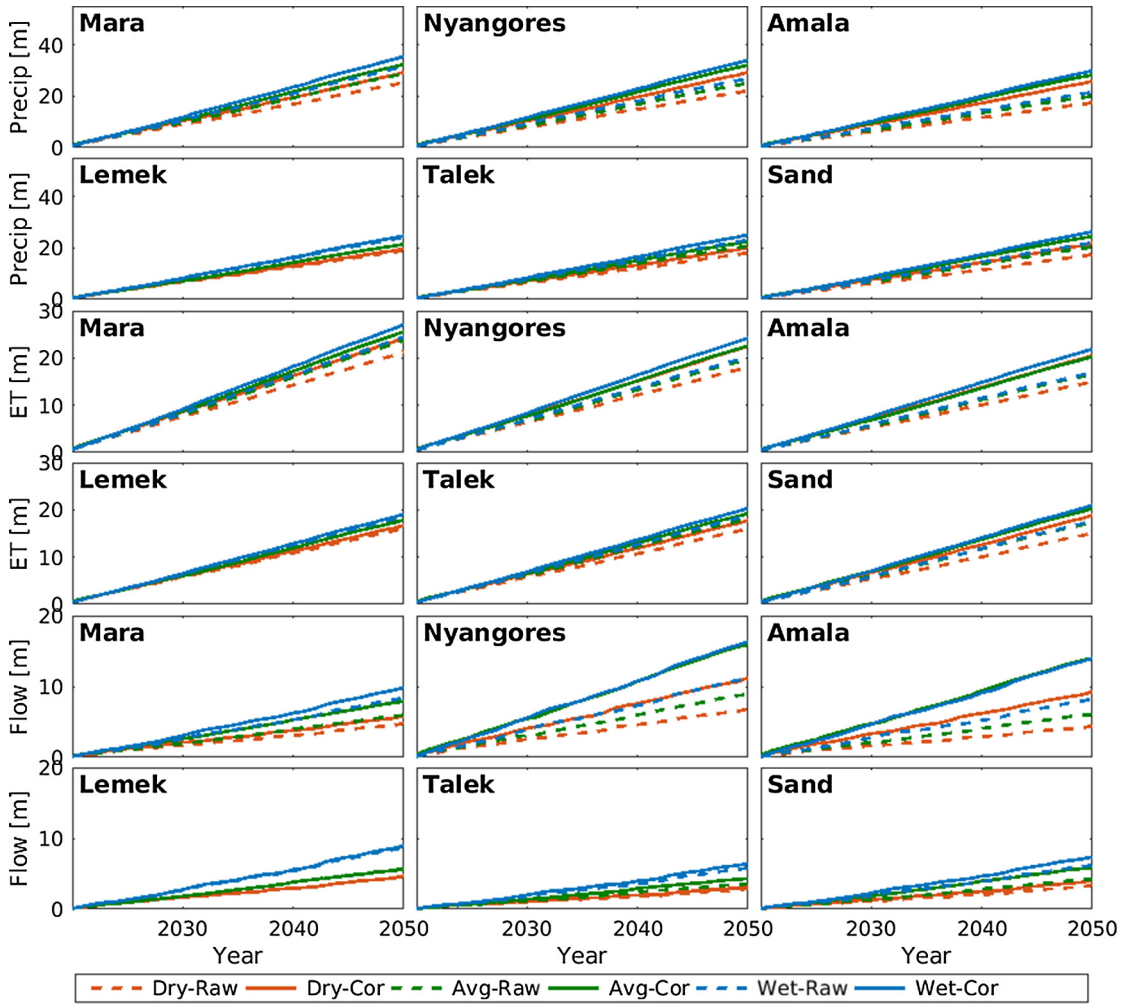

Fig. 6. Accumulated precipitation (m) over the future analysis period (2020–2050) for raw (Raw) and bias-corrected (Cor) scenarios: mean (Avg), 5th percentile (Dry) and 95th percentile (Wet). Bias correction is implemented on the mean scenarios. The anomalies of the dry and wet scenarios are calculated from the raw mean and then added back to the corrected mean to get the corrected dry and wet scenarios.

VIC model, with both raw and bias-corrected future climate precipitation projections, to also study the effects of bias correction. Other variables (maximum temperature, minimum temperature, and wind speed) are used directly from VARAG without any adjustment. With this hydrologic modeling exercise, we want to assess the impacts of short-term/near-term climate change on the hydrology of the Mara River basin. Note that the AgMERRA data used for other variables within the VARAG dataset are already bias-corrected extensively (see Ruane et al., 2015), and therefore their use in the hydrologic model is justified. Future work will focus on bias correcting those variables as well to see if performance could be improved. In this study, we had a reliable reference dataset for precipitation (CHIRPS), which we used to bias-correct the main driver of the hydrologic model, i.e. precipitation.

The average yearly difference between the wet and the dry scenario streamflows was maximum (141 mm) for the Nyangores sub-basin, whereas the minimum difference was found in case of the Sand sub-basin (92 mm). In terms of ET, the maximum difference was found in the overall basin (101 mm) followed by the Talek sub-basin (89 mm), and the minimum in the Amala sub-basins (61 mm).

The effects of bias correction are more prominent for Nyangores and Amala (Figs. 6 and 7). For all three scenarios, VIC simulates streamflows of higher magnitude after the bias correction for these two sub-basins. This behavior is expected, since the corresponding bias factors are also higher (see Supporting Information Fig. S1), meaning that the bias-corrected precipitation would be higher in terms of magnitude as compared to the raw precipitation. The next noticeable change in streamflow is found in case of the Sand sub-basin, which lies in the southern part of the Mara River basin. In this case, the streamflow magnitude increases slightly when the bias-corrected precipitation is used. Streamflow changes are not significant in Lemek and Talek sub-basins.

For the two mountainous sub-basins (Nyangores and Amala), VIC simulation results show that the streamflows for both average and wet scenarios will be very similar (Fig. 6). In other words, streamflow magnitude will be higher, which happens in the expense of ET, since the simulated ET in the average scenario is close to the simulated ET from the dry scenario (lower magnitude). The cumulative distributions of streamflows corresponding to the historical CHIRPS and three VARAG wetness scenarios are shown in Supporting Information Fig. S4.

The distributions of daily precipitation, ET, and streamflow appear to be quite similar in the three successive decades considered in this study (Supporting Information Fig. S5). Although the outliers show some differences, the median and the interquartile range do not change significantly. This is indicative of the fact that at shorter time scales, natural variability of climate can obscure climate change signals.

Being a scenario-based dataset, VARAG shows how different wetness conditions might look like in the future. Thus, Fig. 6 gives us a sense of uncertainty in different hydrologic variables based on the wetness scenarios. Note that since the wetness scenarios are based on seasonal values, after disaggregation using AgMERRA, it is possible to

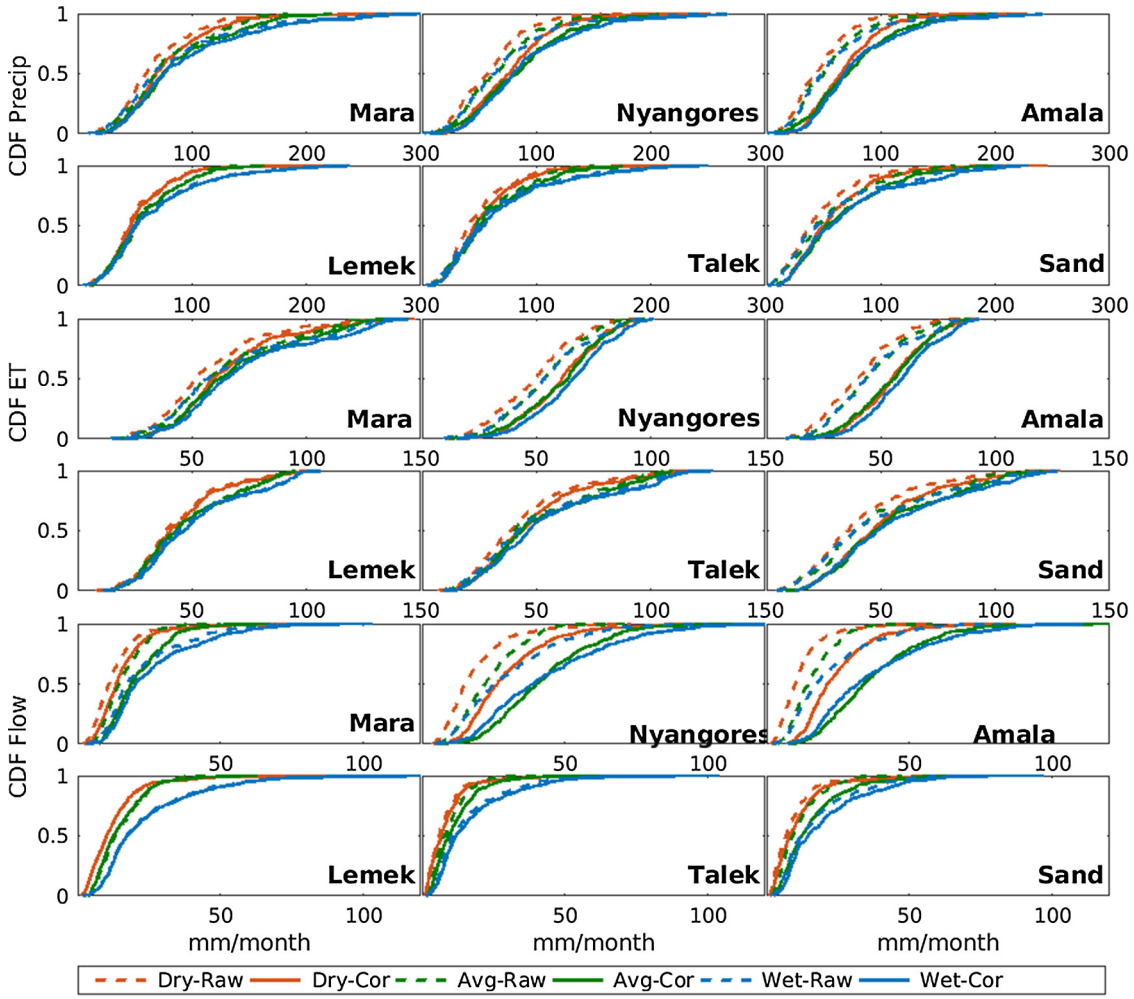

Fig. 7. Empirical cumulative distribution plots of monthly precipitation, evapotranspiration, and streamflows (mm) for different input precipitation scenarios (Dry = 5th percentile; Avg = mean; Wet = 95th percentile) before and after bias correction.

have situations where a daily value from the dry scenario is actually higher than the wet scenario. Therefore, the VARAG scenarios cannot be used directly in the hydrologic model to calculate the corresponding daily streamflow percentiles.

4.5. Trend analysis

Mann-Kendall test at 5% significance level was performed on precipitation, ET, and streamflow during the wet seasons (March-May and October-December) for all three bias-corrected wetness scenarios in the basin. For precipitation, the complete time period (2020–2050) was considered, whereas for ET and streamflows, 2020 was excluded in order to remove the effects of model spin-up.

Except for Sand, the total primary rainy season precipitation (March-May total) showed statistically significant increasing trends for the *average* wetness scenario in all cases, whereas the same scenario did not show any significant trend for the secondary rainy season (October-December total). The *dry* and *wet* scenarios did not show significant trends in any of the sub-basins for either of the rainy seasons. Streamflow did not show any statistically significant trend for any of the rainy seasons and wetness scenarios in any of the sub-basins. For the *average* wetness scenario, increasing trends in ET were found in all cases expect for Sand during the primary rainy season, and in Mara and Lemek during the secondary rainy season. The *wet* scenario did not show any statistically significant trend in ET, whereas, the *dry* scenario showed positive trend during the primary rainy season in Nyangores and Amala. Soil moisture showed statistically significant increasing trends during the primary rainy season in both the *average* and *wet* scenarios for Mara, Nyangores, and Amala (additionally for Lemek in the *average* scenario). However, no statistically significant trend was found in any of the wetness scenarios for annual precipitation, ET, streamflow, and soil moisture, in any of the sub-basins while temperature (both minimum and maximum) showed statistically significant positive annual trends for all the sub-basins. Thus, even with projected increases in seasonal rainfall in some sub-basins and wetness scenarios, they are found to have little influence on the overall hydrology of the basin relative to the current climate when viewed on an annual basis. Increasing ET on an annual time scale (even though the trends are not statistically significant, they are still positive) acts to reduce the runoff, which might not show decreasing trends since the precipitation is also increasing. On subseasonal time scales, increasing temperatures will serve to exacerbate dry conditions when they do occur, even if only driven by natural variability.

We also carried out a comparison between the raw and the bias corrected VARAG precipitation for all three scenarios to see if bias correction is affecting the trend signals in the raw data. It was found that, overall, bias correction did not alter much the temporal trends of the raw data.

4.6. Streamflow uncertainty

Information about streamflow uncertainty is crucial for hydrologic

designs and applications, however, it is almost impossible to get a "true" estimate of uncertainty for the future, simply because we are not certain about how the future would look like in reality. The estimated uncertainties are rather subjective, oftentimes very sensitive to the approach implemented for their estimation. If sufficient computational resources are available, one could calculate an ensemble of streamflow projections, however, the uncertainty thereof (given by the ensemble spread) will be solely based on how good the ensemble members are. Clearly, this approach does not account for the actual errors. Moreover, the uncertainty estimates will change further depending on how the ensemble is generated. An alternative approach to ensemble based uncertainty is to use the historical errors and superimpose them on the future values. The error superimposition can be done for different time scales. In case of daily streamflows, the errors from the entire historical time period could be superimposed on the daily values of the future streamflows. Alternatively, historical errors can be separated into months or even days and the superimposition can be carried out for the corresponding months or days. An important aspect of error calculation is the effect of skewness. In highly skewed variables, such as precipitation or streamflow, the skewness would impact the errors. Therefore, it is important to remove the skewness from the variables before calculating the errors. The error superimposition can be carried out in the transformed space (skewness is reduced), and the resulting streamflow values can then be transferred back to the original space. For long-term assessment, nonstationarity could be an unavoidable issue, in which case, the errors calculated in the past will be irrelevant for the future.

In this study, we first checked if the standard deviations of the daily streamflow errors changed much in the past for each month. Although there were changes evident, it was difficult to find common patterns. Furthermore, it is also problematic to extrapolate the trend line of the historical standard deviations to derive standard deviations for the future, simply because we do not know how that change (whether linear, exponential, etc.) would be in reality. Therefore, in this study, we assumed the streamflow error distributions to be stationary, which is a reasonable assumption, given that our focus is on short-term impacts assessment. Next, we removed the skewness using the Box-Cox transformation, where the "lambda parameter" was calculated such that the skewness was minimized (Roy et al., 2017a, 2017b). We then applied three variations of the error superimposition approach. In Method-1, we superimposed monthly errors, in Method-2, daily error values were used, and finally in Method-3, we applied bootstrapping on the daily errors (Fig. 8). Note that in Method-2 and Method-3, daily error distributions were sparse. For example, in Nyangores River basin, we had 14 years of historical records, resulting in only 14 error values for each day of the year. In most cases, the errors did not have zero-mean. Therefore, we forced the mean to be zero for daily errors to ensure that we capture only the error variance and no artificial bias is introduced in the process. Additionally, in Method-3, instead of regular bootstrapping, we implemented balanced bootstrapping, where the difference between the observation mean and the mean of the bootstrapped sample means are added to the latter to remove the bias.

Note that out of the six sub-basins within the main Mara basin, only three had streamflow observations, with the Nyangores River basin (Station: Bomet Bridge) having the best quality data. Therefore, we demonstrate the streamflow uncertainty analysis for this sub-basin only. For the ungauged basins, an ad-hoc approach of uncertainty characterization would be to use bootstrapped confidence intervals calculated from the daily values in each season. Out of the three methods presented, we recommend the use of Method-1 since it yields to more robust estimates of the uncertainty as the distributions are not sparse in this case, and also, there is no need for forcing the error means to be zero. Method-3 produces the narrowest bounds, however, these are not necessarily more realistic as compared to the more conservative bounds from Method-1. It is important to note that the three wetness scenarios themselves provide a sense of the extreme and mean hydrologic behavior of the basins. The error superimposition, adds an additional layer of uncertainty on the scenarios.

5. Summary and concluding remarks

In this study, we evaluate the potential impacts of short-term (3 decades) climate change on the hydrology of the Mara River basin and its sub-basins in East Africa. Predictability of climate is reduced significantly at such short time span, due to the inherent natural variability. On the other hand, it is oftentimes more relevant to assess the impacts of short-term climate change for water resources management and infrastructure designing. In this study, we capture the natural variability of climate using a statistical model (VAR) and derive daily scenario values based on the AgMERRA data. We bias-correct the new data (VARAG) using the satellite and observation-based merged dataset CHIRPS, and use it as input to the land-surface model VIC to investigate the hydrological impacts. We particularly focus on three different scenarios, representing the mean (avergae), dry (5th percentile), and wet (95th percentile) conditions.

VARAG and AgMERRA have very similar mean bias and distribution characteristics, and they also (along with CHIRPS) well capture the climatology of the bimodal precipitation in the Mara River basin. The bias factors (ratio between reference and raw data) calculated in this study are higher (> 1 indicates underestimation) over the mountainous sub-basins of the north (Nyangores and Amala), agreeing with similar findings about the underestimation of satellite-based precipitation estimates over the mountainous regions (Gebremichael et al., 2014). Therefore, bias correction was more in effect in these two sub-basins. The bias correction method implemented in this study (using kernel densities) successfully matched all four distributional moments of the raw data to that of the reference data. Moreover, it did not alter much the temporal trends of the raw data.

Seasonal trend analysis revealed that the increasing trends in precipitation during the primary rainy season will lead to more water availability, which will not only increase soil moisture but also ET, with the latter also be driven by increasing temperatures. Annually, there is no substantial increase in precipitation in the next three decades as shown by the VARAG data (CMIP5 model outputs combined with natural variability), which relates to the frequent drought events in the region. Another implication of these results could be that the primary rainy season in the sub-basins (for most of them) will have more rain, however, since the overall annual precipitation is not changing much, this could lead to higher peak flows during the rainy seasons (not necessarily increased total flow) and more dryness during the non-rainy seasons, which have been suggested in some recent studies (e.g. Mati et al., 2008; Mango et al., 2011).

It should be noted that in our study approach, projected rainfall trends from the CMIP5 models are for seasonal totals that are superimposed on natural variability on this time scale and subsequently disaggregated to daily sequences using the AgMERRA dataset. As such, we do not explicitly examine changes in daily extreme events within the CMIP5 models, although seasonal rainfall trends will influence the magnitude of daily totals, including extremes, in our approach. Our methodology assumes that in the near term (10–30 years), climate variability will be very similar to that of the present climate, which may not be a suitable assumption on longer timescales under increasing greenhouse gas forcing. Given this, our methodology is not ideal for the analysis of daily rainfall trends. The strength of the VAR approach is to allow for the generation of thousands of plausible future climate scenarios, enabling us to build probability distributions of projected climate change that include the important role of unforced climate variability on near term trends.

Acknowledgement

This work was supported by the NASA-USAID SERVIR Program

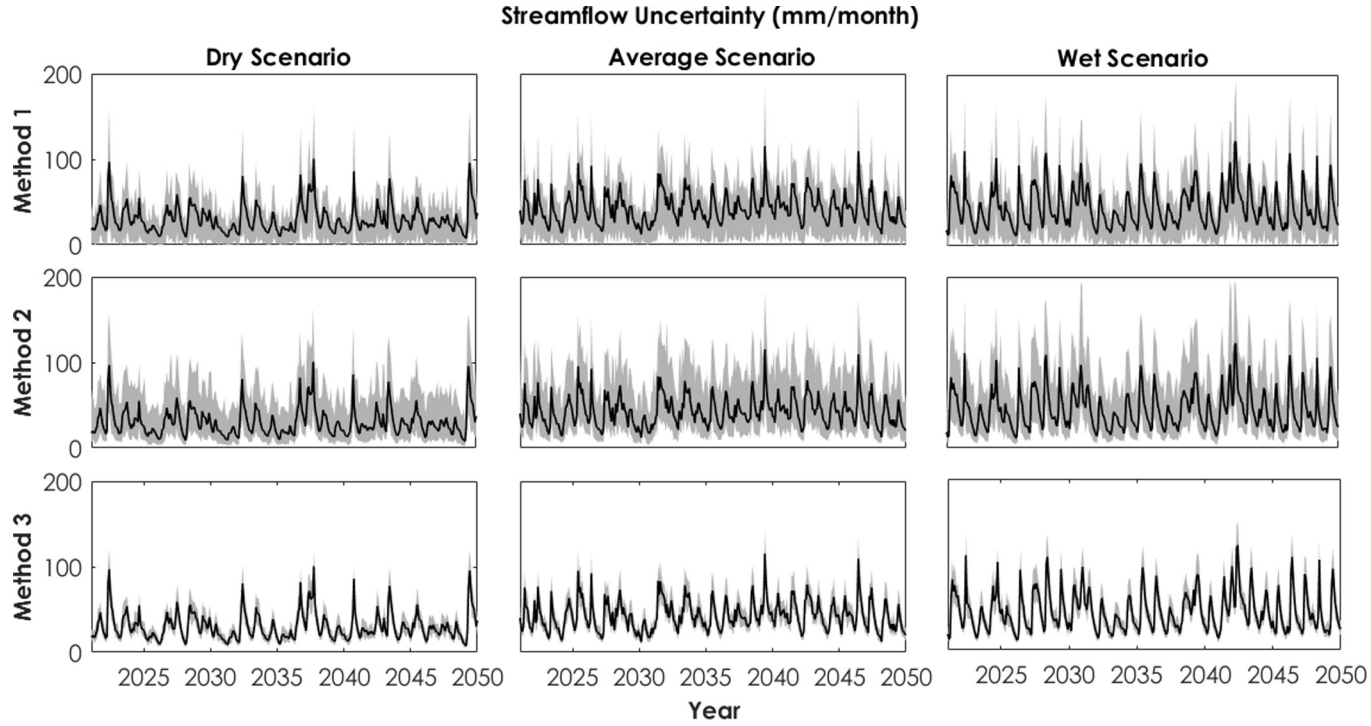

Fig. 8. Streamflow uncertainty based on historical errors. Units are in mm/month.

through award 11-SERVIR11-58. Thanks to Ashutosh Limaye and the entire SERVIR Applied Sciences Team for their valuable feedback throughout the course of the project. Michael McClain, Eric Kabuchanga, and Faith Mitheu provided great help in obtaining historical streamflow observations and liaising with national and local water managers. Thanks to Michael Bell and John del Corral from the International Research Institute for Climate and Society, Columbia University, for their assistance in acquiring the AgMERRA data. Additional information about the results presented in this study are available upon request from the corresponding author, Tirthankar Roy (royt@email.arizona.edu).

Conflicts of interest

The authors express no conflicts of interests.

Appendix A. Supplementary data

Supplementary data associated with this article can be found, in the online version, at https://doi.org/10.1016/j.jhydrol.2018.08.051.

References

Allen, M., Frame, D., Kettleborough, J., Stainforth, D., 2006. Model error in weather and climate forecasting. In: Palmer, T., Hagedorn, R. (Eds.), Predictability of Weather and Climate. Cambridge University Press, Cambridge, pp. 391–427. https://doi.org/10.1017/CBO9780511617652.016.

Boer, G.J., Lambert, S.J., 2008. Multi-model decadal potential predictability of precipitation and temperature. Geophys. Res. Lett. 35, L05706. https://doi.org/10.1029/2008GL033234.

Box, G.E.P., Cox, D.R., 1964. An analysis of transformations. J. R. Stat. Soc. Ser. B 26, 211–252.

Chen, M., Shi, W., Xie, P., Silva, V.B.S., Kousky, V.E., Wayne Higgins, R., Janowiak, J.E., 2008. Assessing objective techniques for gauge-based analyses of global daily precipitation. J. Geophys. Res. 113, D04110. https://doi.org/10.1029/2007JD009132.

Defersha, M.B., Melesse, A.M., McClain, M.E., 2012. Watershed scale application of WEPP and EROSION 3D models for assessment of potential sediment source areas and runoff flux in the Mara River Basin, Kenya. CATENA 95, 63–72. https://doi.org/10.1016/j.catena.2012.03.004.

Dessu, S.B., Melesse, A.M., 2012. Impact and uncertainties of climate change on the hydrology of the Mara River basin Kenya/Tanzania. Hydrol. Process. 27, 2973–2986. https://doi.org/10.1002/hyp.9434.

Dessu, S.B., Melesse, A.M., Bhat, M.G., McClain, M.E., 2014. Assessment of water resources availability and demand in the Mara River Basin. CATENA 115, 104–114. https://doi.org/10.1016/j.catena.2013.11.017.

Duan, Q., Sorooshian, S., Gupta, V., 1992. Effective and efficient global optimization for conceptual rainfall-runoff models. Water Resour. Res. 28, 1015–1031. https://doi.org/10.1029/91WR02985.

Duan, Q.Y., Gupta, V.K., Sorooshian, S., 1993. Shuffled complex evolution approach for effective and efficient global minimization. J. Optim. Theory Appl. 76, 501–521.

Dunn, R.J.H., Willett, K.M., Thorne, P.W., Woolley, E.V., Durre, I., Dai, A., Parker, D.E., Vose, R.S., 2012. HadISD: a quality-controlled global synoptic report database for selected variables at long-term stations from 1973–2011. Clim. Past 8, 1649–1679. https://doi.org/10.5194/cp-8-1649-2012.

Flato, G., Marotzke, J., Abiodun, B., Braconnot, P., Chou, S.C., Collins, W., Cox, P., Driouech, F., Emori, S., Eyring, V., Forest, C., Gleckler, P., Guilyardi, E., Jakob, C., Kattsov, V., Reason, C., Rummukainen, M., 2013. Evaluation of climate models. In: Stocker, T.F., Qin, D., Plattner, G.-K., Tignor, M., Allen, S.K., Boschung, J., Nauels, A., Xia, Y., Bex, V., Midgley, P.M. (Eds.), Climate Change 2013: The Physical Science Basis. Contribution of Working Group I to the Fifth Assess- Ment Report of the Intergovernmental Panel on Climate Change. Cambridge University Press, Cambridge, United Kingdom and New York, NY, USA.

Funk, C., Peterson, P., Landsfeld, M., Pedreros, D., Verdin, J., Shukla, S., Husak, G., Rowland, J., Harrison, L., Hoell, A., Michaelsen, J., 2015. The climate hazards infrared precipitation with stations—a new environmental record for monitoring extremes. Sci. Data 2, 150066. https://doi.org/10.1038/sdata.2015.66.

Funk, C.C., Peterson, P.J., Landsfeld, M.F., Pedreros, D.H., Verdin, J.P., Rowland, J.D., Romero, B.E., Husak, G.J., Michaelsen, J.C., Verdin, A.P., 2014. A quasi-global precipitation time series for drought monitoring. U.S. Geological Survey Data Series. https://doi.org/10.3133/ds832.

Gebremichael, M., Bitew, M.M., Hirpa, F.A., Tesfay, G.N., 2014. Accuracy of satellite rainfall estimates in the Blue Nile Basin: lowland plain versus highland mountain. Water Resour. Res. 50, 8775–8790. https://doi.org/10.1002/2013WR014500.

Greene, A.M., Goddard, L., Cousin, R., 2011. Web tool deconstructs variability in twentieth-century climate. Eos Trans. AGU 92 (45), 397–398. https://doi.org/10.1029/2011EO450001.

Greene, A.M., Hellmuth, M., Lumsden, T., 2012. Stochastic decadal climate simulations for the Berg and Breede Water Management Areas, Western Cape province South Africa. Water Resour. Res. 48, 1–13. https://doi.org/10.1029/2011WR011152.

Gupta, H.V., Clark, M.P., Vrugt, J.A., Abramowitz, G., Ye, M., 2012. Towards a comprehensive assessment of model structural adequacy. Water Resour. Res. 48, W08301. https://doi.org/10.1029/2011WR011044.

Harris, I., Jones, P.D., Osborn, T.J., Lister, D.H., 2014. Updated high-resolution grids of monthly climatic observations - the CRU TS3.10 Dataset. Int. J. Climatol. 34, 623–642. https://doi.org/10.1002/joc.3711.

Hsu, K., Gao, X., Sorooshian, S., Gupta, H.V., 1997. Precipitation estimation from remotely sensed information using artificial neural networks. J. Appl. Meteorol. 36, 1176–1190. https://doi.org/10.1175/1520-0450(1997) 036<1176:PEFRSI>2.0.CO;2.

Huffman, G.J., Bolvin, D.T., Nelkin, E.J., Wolff, D.B., Adler, R.F., Gu, G., Hong, Y.,

Bowman, K.P., Stocker, E.F., 2007. The TRMM multisatellite precipitation analysis (TMPA): quasi-global, multiyear, combined-sensor precipitation estimates at fine scales. J. Hydrometeorol. 8, 38–55. https://doi.org/10.1175/JHM560.1.

Iizumi, T., Okada, M., Yokozawza, M., 2014. A meteorological forcing data set for global crop modeling: development, evaluation, and intercomparison. J. Geophys. Res. Atmos. 119, 363–384. https://doi.org/10.1002/2013JD020130.

Joyce, R.J., Janowiak, J.E., Arkin, P.A., Xie, P., 2004. CMORPH: a method that produces global precipitation estimates from passive microwave and infrared data at high spatial and temporal resolution. J. Hydrometeorol. 5, 487–503. https://doi.org/10.1175/1525-7541(2004)005<0487:CAMTPG>2.0.CO;2.

Kim, T.-W., Valdés, J.B., Yoo, C., 2003. Nonparametric approach for estimating return periods of droughts in arid regions. J. Hydrol. Eng. 8, 237–246. https://doi.org/10.1061/(ASCE)1084-0699(2003) 8:5(237).

Liang, X., Lettenmaier, D.P., Wood, E.F., Burges, S.J., 1994. A simple hydrologically based model of land surface water and energy fluxes for general circulation models. J. Geophys. Res. 99, 14415. https://doi.org/10.1029/94JD00483.

Lohmann, D., Nolte-Holube, R., Raschke, E., 1996. A large-scale horizontal routing model to be coupled to land surface parametrization schemes. Tellus A 48, 708–721. https://doi.org/10.1034/j.1600-0870.1996.t01-3-00009.x.

Lohmann, D., Rashke, E., Nijssen, B., Lettenmaier, D.P., 1998. Regional scale hydrology: I. Formulation of the VIC-2L model coupled to a routing model. Hydrol. Sci. J. 43, 131–141. https://doi.org/10.1080/02626669809492107.

Lyon, B., Vigaud, N., 2017. Unraveling East Africa's climate paradox. In: Wang, S.-Y. (Ed.), Patterns of Climate Extremes: Trends and Mechanisms. John Wiley and American Geophysical Union, Hoboken, NJ and Washington, DC, pp. 265–281.

Mango, L.M., Melesse, A.M., McClain, M.E., Gann, D., Setegn, S.G., 2011. Land use and climate change impacts on the hydrology of the upper Mara River Basin, Kenya: results of a modeling study to support better resource management. Hydrol. Earth Syst. Sci. 15, 2245–2258. https://doi.org/10.5194/hess-15-2245-2011.

Mati, B.M., Mutie, S., Gadain, H., Home, P., Mtalo, F., 2008. Impacts of land-use/cover changes on the hydrology of the transboundary Mara River Kenya/Tanzania. Lakes Reserv. Res. Manag. 13, 169–177. https://doi.org/10.1111/j.1440-1770.2008.00367.x.

Mati, B.M., Mutie, S., Home, P., Mtalo, F., Gadain, H., 2005. Land use changes in the transboundary mara basin: A threat to pristine wildlife sanctuaries in East Africa. In A Paper presentation at the: 8th International River Symposium, Brisbane, Australia (pp. 6-9)., in: 8th International River Symposium, Brisbane, Australia.

McClain, M.E., Subalusky, A.L., Anderson, E.P., Dessu, S.B., Melesse, A.M., Ndomba, P.M., Mtamba, J.O.D., Tamatamah, R.A., Mligo, C., 2014. Comparing flow regime, channel hydraulics, and biological communities to infer flow–ecology relationships in the Mara River of Kenya and Tanzania. Hydrol. Sci. J. 59, 801–819. https://doi.org/10.1080/02626667.2013.853121.

Panofsky, H.W., Brier, G.W., 1968. Some Applications of Statistics to Meteorology. PA. State Univ. Press, University Park.

Reichle, R.H., 2012. The MERRA-land data product (Version 1.2).

Riahi, K., Rao, S., Krey, V., Cho, C., Chirkov, V., Fischer, G., Kindermann, G., Nakicenovic, N., Rafaj, P., 2011. RCP 8.5—A scenario of comparatively high greenhouse gas emissions. Clim. Change 109, 33–57. https://doi.org/10.1007/s10584-011-0149-y.

Rienecker, M.M., Suarez, M.J., Gelaro, R., Todling, R., Bacmeister, J., Liu, E., Bosilovich, M.G., Schubert, S.D., Takacs, L., Kim, G.-K., Bloom, S., Chen, J., Collins, D., Conaty, A., da Silva, A., Gu, W., Joiner, J., Koster, R.D., Lucchesi, R., Molod, A., Owens, T., Pawson, S., Pegion, P., Redder, C.R., Reichle, R., Robertson, F.R., Ruddick, A.G., Sienkiewicz, M., Woollen, J., 2011. MERRA: NASA's Modern-era retrospective analysis for research and applications. J. Clim. 24, 3624–3648. https://doi.org/10.1175/JCLI-D-11-00015.1.

Rosenblatt, M., 1956. Remarks on some nonparametric estimates of a density function. Ann. Math. Stat. 27, 823–837.

Roy, T., Gupta, H.V., Serrat-Capdevila, A., Valdes, J.B., 2017a. Using satellite-based evapotranspiration estimates to improve the structure of a simple conceptual rainfall-runoff model. Hydrol. Earth Syst. Sci. 21, 879–896. https://doi.org/10.5194/hess-21-879-2017.

Roy, T., Serrat-Capdevila, A., Gupta, H., Valdes, J., 2017b. A platform for probabilistic multimodel and multiproduct streamflow forecasting. Water Resour. Res. 53. https://doi.org/10.1002/2016WR019752.

Ruane, A.C., Goldberg, R., Chryssanthacopoulos, J., 2015. Climate forcing datasets for agricultural modeling: Merged products for gap-filling and historical climate series estimation. Agric. For. Meteorol. 200, 233–248. https://doi.org/10.1016/j.agrformet.2014.09.016.

Sheather, S.J., Jones, M.C., 1991. A Reliable Data-Based Bandwidth Selection Method for Kernel Density Estimation. J. R. Stat. Soc. Ser. B 53, 683–690.

Sheffield, J., Goteti, G., Wood, E.F., 2006. Development of a 50-Year High-resolution global dataset of meteorological forcings for land surface modeling. J. Clim. 19, 3088–3111. https://doi.org/10.1175/JCLI3790.1.

Silverman, B.W., 1981. Using kernel density estimates to investigate multimodality. J. R. Stat. Soc. Ser. B 43, 97–99.

Snover, A.K., Hamlet, A.F., Lettenmaier, D.P., 2003. Climate-change scenarios for water planning studies: pilot applications in the pacific northwest. Bull. Am. Meteorol. Soc. 84, 1513–1518. https://doi.org/10.1175/BAMS-84-11-1513.

Taylor, K.E., Stouffer, R.J., Meehl, G.A., 2012. An overview of CMIP5 and the experiment design. Bull. Am. Meteorol. Soc. 93, 485–498. https://doi.org/10.1175/BAMS-D-11-00094.1.

Teng, H., Branstator, G., 2011. Initial-value predictability of prominent modes of North Pacific subsurface temperature in a CGCM. Clim. Dyn. 36, 1813–1834. https://doi.org/10.1007/s00382-010-0749-7.

Teutschbein, C., Seibert, J., 2012. Bias correction of regional climate model simulations for hydrological climate-change impact studies: review and evaluation of different methods. J. Hydrol. 456–457, 12–29. https://doi.org/10.1016/j.jhydrol.2012.05.052.

Teutschbein, C., Wetterhall, F., Seibert, J., 2011. Evaluation of different downscaling techniques for hydrological climate-change impact studies at the catchment scale. Clim. Dyn. 37, 2087–2105. https://doi.org/10.1007/s00382-010-0979-8.

Weedon, G.P., Gomes, S., Viterbo, P., Shuttleworth, W.J., Blyth, E., Österle, H., Adam, J.C., Bellouin, N., Boucher, O., Best, M., 2011. Creation of the WATCH forcing data and its use to assess global and regional reference crop evaporation over land during the twentieth century. J. Hydrometeorol. 12, 823–848. https://doi.org/10.1175/2011JHM1369.1.

Wood, A.W., Maurer, E.P., Kumar, A., Lettenmaier, D.P., 2002. Long-range experimental hydrologic forecasting for the eastern United States. J. Geophys. Res. 107, 4429. https://doi.org/10.1029/2001JD000659.

Yang, W., Seager, R., Cane, M.A., Lyon, B., 2014. The east African long rains in observations and models. Journal of Climate 27 (19), 7185–7202.

Yang, W., Seager, R., Cane, M.A., Lyon, B., 2015. The rainfall annual cycle bias over East Africa in CMIP5 coupled climate models. J. Clim. 28 (24), 9789–9802.

Yuan, X., Wood, E.F., 2012. Downscaling precipitation or bias-correcting streamflow? Some implications for coupled general circulation model (CGCM)-based ensemble seasonal hydrologic forecast. Water Resour. Res. 48, W12519. https://doi.org/10.1029/2012WR012256.